Theor Appl Climatol (2015) 120:123–135
DOI 10.1007/s00704-014-1162-7

ORIGINAL PAPER

A numerical study of the interactions of urban breeze circulation with mountain slope winds

Gantuya Ganbat · Jong-Jin Baik · Young-Hee Ryu

Received: 11 December 2013 / Accepted: 14 April 2014 / Published online: 2 May 2014

Abstract The two-dimensional interactions of urban breeze circulation with mountain slope winds are investigated using the Weather Research and Forecasting (WRF) model coupled with the Seoul National University Urban Canopy Model (SNUUCM). A city is located near an isolated mountain, and there is no basic-state wind. Circulation over the urban area is asymmetric and characterized by the weakened mountain-side urban wind due to the opposing upslope wind and the strengthened plain-side urban wind in the daytime. The transition from upslope wind to downslope wind on the urban-side mountain slope occurs earlier than that on the mountain slope in a simulation that includes only an isolated mountain. A hydraulic jump occurs in the late afternoon, when the strong downslope wind merges with weaker mountain-side urban wind and stagnates until late evening. The sensitivities of the interactions of urban breeze circulation with mountain slope winds and urban heat island intensity to mountain height and urban fraction are also examined. As mountain height decreases and urban fraction increases, the transition from urban-side upslope wind to downslope wind occurs earlier and the urban-side downslope wind persists longer. This change in transition time from urban-side upslope wind to downslope wind affects the interactions between urban breeze circulation and mountain slope winds. Urban heat island intensity is more sensitive to urban fraction than to mountain height. Each urban fraction increase of 0.1 results in an average increase of 0.17 °C (1.27 °C) in the daytime (nighttime) urban heat island intensity. A simulation in which a city is located in a basin shows that the urban-side downslope wind develops earlier, persists longer, and is stronger than in the simulation that includes a city and an isolated mountain.

G. Ganbat · J.-J. Baik (✉) · Y.-H. Ryu
School of Earth and Environmental Sciences,
Seoul National University, Seoul 151-742, South Korea
e-mail: jjbaik@snu.ac.kr

Y.-H. Ryu
Department of Civil and Environmental Engineering,
Princeton University, Princeton, NJ 08544, USA

1 Introduction

Many interesting thermally induced wind systems occur locally, including sea/land breezes, mountain/valley winds (or downslope/upslope winds), lake breezes, and urban breezes. Of these local wind systems, sea/land breezes, mountain/valley winds, and lake breezes have been investigated extensively through observational, theoretical, and numerical modeling studies (Simpson 1994; Pielke 2002). However, urban breezes have been less investigated despite the important roles urban breezes play in local weather and air quality (Ryu et al. 2013a).

Urban breeze circulation (also known as urban heat island circulation) is induced by the difference in near-surface air temperature between the urban area and its surrounding rural area, that is, the urban heat island. Urban breeze circulation has been observed in many cities (Wong and Dirks 1978; Hidalgo et al. 2008b) and has been simulated numerically (Lemonsu and Masson 2002; Hidalgo et al. 2008a; Ryu and Baik 2013). These previous studies indicate that urban breeze circulation is characterized by inward flow toward the city center in the lower boundary layer, upward motion near the city center, outward flow toward the surrounding rural area in the upper boundary layer, and weak downward motion outside and that urban breeze circulation is stronger in the daytime than in the nighttime. For example, the boundary layer simulated over the Paris area in France was deeper in the daytime than in the nighttime, with converging (diverging) flow of 5–7 m s^{-1} at lower (upper) levels and upward vertical velocities of ~1 m s^{-1} (Lemonsu and Masson 2002).

When a city is located near mountains, both the urban breeze and upslope/downslope winds are thermally induced and interact with each other. Previous numerical modeling studies have investigated wind modifications in the presence of urban areas and topography or interactions between the urban breeze and upslope/downslope winds. Savijarvi and Liya (2001) examined local winds around a valley city through idealized two-dimensional simulations. They found the daytime urban breeze circulation to oppose the weak daytime upslope circulation of a narrow valley, resulting in relatively weak daytime winds. Conversely, the nighttime downslope wind wipes out the weak nighttime urban breeze circulation, resulting in purely katabatic winds in the nighttime and morning. Ohashi and Kida (2002) examined the effects of mountains and urban areas on daytime local circulations in the Osaka and Kyoto regions in Japan. Their results demonstrated that valley circulation weakens the urban breeze circulation and causes surface air temperatures to increase through adiabatic warming by subsidence. Lee and Kim (2010) performed idealized two-dimensional simulations and showed that the urban sensible heat flux acts to accelerate nocturnal drainage flow, which tends to increase the return flow above. Ryu and Baik (2013) simulated local circulations in the Seoul metropolitan area in South Korea and demonstrated that the upslope wind turns to downslope wind and the downslope wind strengthens with gradual strengthening of the urban breeze circulation in the daytime. These modeling studies provide valuable insights into interactions between urban breeze circulation and upslope/downslope winds.

Many factors, including urban fraction and urban surface roughness, affect the intensity of urban breeze circulation, and mountain shape and height influence upslope/downslope wind speeds. Thus, the degree of interactions between urban breeze circulation and upslope/downslope winds depends on such factors. The present study investigates the interactions of urban breeze circulation with upslope/downslope winds and the dependences of these interactions and urban heat island intensity on mountain height and urban fraction using a mesoscale model coupled with an advanced urban canopy model. Idealized two-dimensional simulations are conducted to clearly understand these interactions and these dependences within a simple framework.

In Section 2, the numerical model used and the experimental design are described. The simulation results are presented and discussed in Section 3. Summary and conclusions are provided in Section 4.

2 Model description and experimental design

The numerical model adopted in the present study is the Weather Research and Forecasting (WRF) model version 3.2 (Skamarock et al. 2008) coupled with the Seoul National University Urban Canopy Model (SNUUCM) (Ryu et al. 2011). The model physics options are as follows: the Yonsei University (YSU) planetary boundary layer scheme (Hong et al. 2006), the Rapid Radiative Transfer Model (RRTM) longwave radiation scheme (Mlawer et al. 1997), the Dudhia shortwave radiation scheme (Dudhia 1989), and the Purdue Lin cloud microphysics scheme (Chen and Sun 2002). The SNUUCM parameterizes important physical processes that occur in urban canopies, including absorption and reflection of shortwave and longwave radiation, turbulent energy and water exchanges between surfaces (road, two facing walls, and roof) and adjacent air, and conductive heat transfer through substrates (Ryu et al. 2011). The SNUUCM is coupled with the Noah Land Surface Model (Chen and Dudhia 2001) in a tile approach. The WRF model coupled with the SNUUCM has been applied previously to investigate local circulations and urban impacts on air quality in the Seoul metropolitan area (Ryu et al. 2013b; Ryu and Baik 2013).

A city and an isolated mountain are considered to examine two-dimensional interactions between urban breeze circulation and mountain slope winds. The city has a size of 20 km, and the urban area consists of built-up (80 %) and natural (20 %) areas. All natural areas consist of cropland–woodland mosaic (60 %) and loamy soil sand (40 %). Some important urban parameters in the SNUUCM are specified as follows: the roof level height is 15 m, the canyon aspect ratio is 1, and the emissivity and albedo of all artificial surfaces (road, wall, and roof) are 0.95 and 0.2, respectively. The mountain is Gaussian-shaped with a size of 20 km, which is given by $h(x) = h_m e^{-\left(\frac{x-c}{k}\right)^2}$, where h_m is the maximum mountain height, c is the horizontal location of the mountain peak, and k is the slope parameter (k=5,000 m).

The domain size is 200 km in the horizontal and 8 km in the vertical. The horizontal grid interval is 500 m. The vertical grid interval is stretched with height, with the lowest model level being z=48 m, and the number of vertical layers is 82. The Rayleigh damping layer is set to z=6–8 km to avoid the reflection of waves at the top of the physical domain (z=6 km). The lateral boundary condition is periodic. The mountain height is set to zero at mountain-edge grid points. The initial potential temperature at the surface is 298 K, and the lapse rate of the initial potential temperature is 5 K km^{-1}. No basic-state wind is considered to ensure that focus is placed on thermally induced circulation/flow. The initial relative humidity is uniform throughout z=0–4 km (30 %), decreases linearly with height up to z=6 km (where it is 10 %), and remains constant above this height. Since this study is concerned with thermally induced local circulations, the initial relative humidity is set to be low so that clouds and precipitation do not occur. The effect of Earth's rotation is neglected, and the latitude is set to 30° N. The model is integrated for 27 h starting from 0500 LST on June 23, and the 24-h simulation data starting from 0800 LST are used for analysis.

3 Results and discussion

3.1 Urban breeze circulation and mountain slope winds

In this section, the simulated general features of urban breeze circulation and mountain slope winds are presented in brief. Figure 1 shows the horizontal velocity, vertical velocity, and velocity vector fields and the potential temperature anomaly field at 0900, 1300, 1900, and 2300 LST in a simulation that includes only a city (hereafter, the URBAN simulation). The potential temperature anomaly is calculated as the difference between total and horizontally averaged values at each height. The city spans x=100–120 km. The urban breeze circulation is induced by the horizontal temperature difference between the urban area and the surrounding rural area.

At 0900 LST, a weak horizontal potential temperature difference is present and an urban breeze circulation is about to form. As the horizontal temperature difference increases with time, the urban breeze circulation becomes well established. The urban breeze circulation is symmetric about the urban center (x=110 km) because there is no basic-state wind. At 1300 LST, urban breeze fronts are located at x=105 and 115 km and the horizontal wind behind the urban breeze fronts is strong. The two urban breeze fronts move toward the

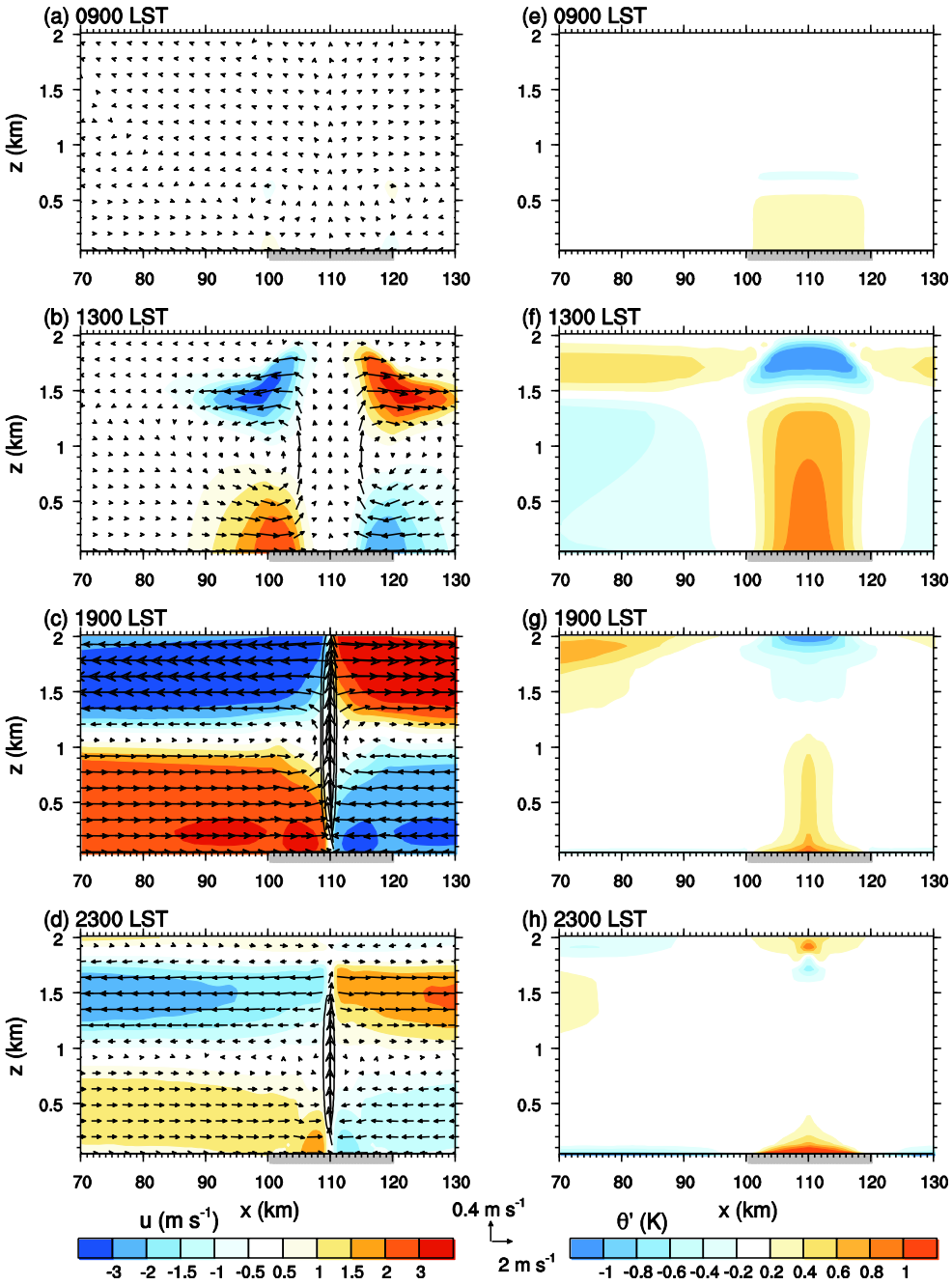

Fig. 1 Horizontal velocity (*shading*), vertical velocity (*contour*), and velocity vector fields at **a** 0900, **b** 1300, **c** 1900, and **d** 2300 LST and corresponding potential temperature anomaly field (*shading*) at **e** 0900, **f** 1300, **g** 1900, and **h** 2300 LST in the URBAN simulation. The *gray box on the x-axis* indicates the urban area. The contour levels of vertical velocity are 0.5, 1, and 2 m s^{-1}

urban center, colliding with each other around 1455 LST and subsequently merging to produce strong upward motion. At 1900 LST, a strong updraft cell centered at the urban center appears, with a maximum updraft intensity of 2.0 m s^{-1} at z=1,150 m. Note that 1900 LST is very close to the sunset time on June 23 (~1858 LST). The urban breeze circulation is stronger in the late afternoon/early evening than in the early afternoon (Fig. 1b, c). This is consistent with the result of Savijarvi and Liya (2001). The simulated urban breeze circulation is characterized by converging flow in the lower layer and diverging flow in the upper layer (Fig. 1b, c). At 1300 and 1900 LST, deeper urban boundary layer results in the negative (cold) potential temperature anomaly in the upper layer owing to higher potential temperature in the rural area than in the urban area at the same upper level because of strong stratification above the top of rural boundary layer (Fig. 1f, g). The horizontal size of the urban breeze circulation at 1300 (1900) LST is 2.0 (3.9) times as large as the urban size. This is similar to the results of Hidalgo et al. (2008a) and Ryu et al. (2013a). The vertical size of the urban breeze circulation is ~1.8 km at 1300 LST and ~2.2 km at 1900 LST. It is notable that the horizontal and vertical sizes of the urban breeze circulation vary considerably with time. In the nighttime, although the near-surface potential temperature difference between the urban area and the surrounding rural area is relatively large (i.e., larger nighttime urban heat island), the urban breeze circulation is weak owing to nighttime stable stratification that suppresses vertical motion (Fig. 1d).

A simulation with Earth's rotation was performed with flat terrain and a city being considered, and simulation results were compared with the results of the simulation without Earth's rotation (that is, the URBAN simulation). In both the simulations, daytime urban breeze circulations are similar to each other. When the Earth's rotation is included, in the late evening, winds start to turn away from the city above the surface, exhibiting an anti-urban heat island circulation-like feature (Savijarvi and Liya 2001). The transverse wind (v velocity) arises in the simulation with Earth's rotation due to the Coriolis force, but in the daytime its magnitude is smaller than that of u velocity.

Figure 2 shows the horizontal velocity, vertical velocity, and velocity vector fields and the potential temperature anomaly field at 0900, 1300, 1900, and 2300 LST in a simulation that includes only a mountain (hereafter, the MOUNT simulation). In this simulation, the mountain peak is located at x=90 km, and the maximum mountain height (h_m) is 500 m. As expected, the upslope (downslope) wind appears at 0900 and 1300 (1900 and 2300) LST. Note that the downslope wind at 1900 LST occurs near the mountain slope surface. At 1300 LST, a strong updraft cell is produced over the mountain top and flow in the upper layer diverges away from the mountain, forming an apparent mountain circulation. Above the mountain top, a weak warm region and a relatively strong cold region are observed. The upslope wind attains a maximum intensity of 2.2 m s^{-1} around 1340 LST. The transition from upslope wind to downslope wind at a midslope location (x=95 km) occurs around 1845 LST. During the 24-h period, the occurrence frequency of the 10-m upslope wind at the midslope location (47 %) is similar to that of the downslope wind (53 %).

3.2 Interactions of urban breeze circulation with mountain slope winds

To examine interactions between urban breeze circulation and mountain slope winds, a numerical experiment in which both a city and a mountain exist is performed. This simulation is referred to as the URBAN-MOUNT simulation. The horizontal size of the city (20 km) is the same as that of the mountain, and the horizontal location of the mountain peak (urban center) is x=90 (110) km. The maximum mountain height is set to 500 m. Several terms are utilized in the present study to indicate areas or locations within the domain. The mountain slope on the rural (urban) side is referred to as the rural-side (urban-side) mountain slope and spans x=80–90 (90–100) km (Fig. 3). The urban area whose edge borders the mountain (plain) area is referred to as the mountain-side (plain-side) urban area and spans x=100–110 (110–120) km. The urban periphery that borders the mountain (rural) area is referred to as the mountain–urban (urban–rural) edge [x=100 (120) km]. In the URBAN-MOUNT simulation, the mountain–urban edge is located at the center of the domain.

Figure 3 shows the horizontal velocity, vertical velocity, and velocity vector fields and the potential temperature anomaly field at five different times (1300, 1500, 1600, 1900, and 2300 LST) in the URBAN-MOUNT simulation. At 1300 LST, the upslope wind on the mountain slope and an updraft cell over the mountain top are produced. The upslope wind is stronger on the rural-side mountain slope than on the urban-side mountain slope because the mountain upslope wind on the urban-side mountain slope is opposed by the urban breeze. The circulation over the urban area is not symmetric about the urban center owing to the influence of the mountain circulation. At 1500 LST, the upslope wind exists on the rural-side mountain slope, whereas the downslope wind exists in the lower region of the urban-side mountain slope. Two updraft cells over the urban area are apparent and are associated with urban breeze fronts. The updraft cell centered at x=105.5 km is influenced more by the mountain circulation than that centered at x=109.5 km. A deep warm region centered at x=105.5 km is formed (Fig. 3g). The two updraft cells move toward each other, colliding around 1540 LST and subsequently merging to produce a strong updraft cell. At 1600 LST, the downslope wind on the urban-side mountain slope is produced and the two updraft cells are merged into a strong updraft cell centered at x=106.5 km. The plain-side urban

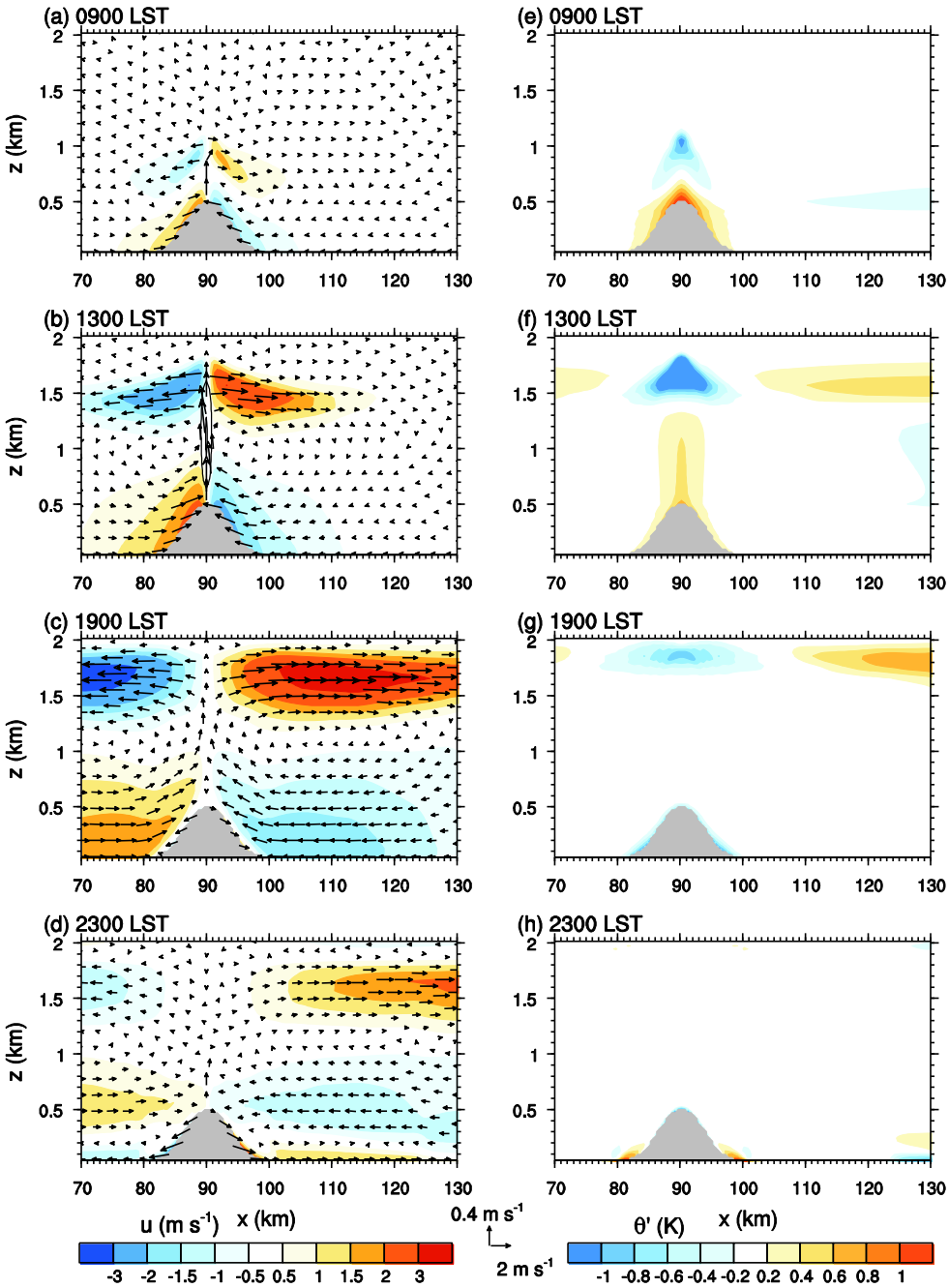

Fig. 2 Same as in Fig. 1 but for the MOUNT simulation. The contour levels of vertical velocity are 0.5 and 1 m s^{-1}

wind pushes the urban breeze convergence zone toward the mountain. At 1900 LST, the downslope wind on the urban-side mountain slope is enhanced. At 2300 LST, the downslope wind is present on both sides of the mountain, the urban wind weakens, and a shallow warm region is observed over the urban area. In this study, night–morning transitions and circulations are not focused, but they deserve an investigation with a longer time simulation.

Fernando (2010) noted that downslope flow approaching a slope break may undergo hydraulic adjustment and then merge with the urban nocturnal atmospheric boundary layer. In the URBAN-MOUNT simulation, a clear hydraulic jump appears at 1900 LST (Fig. 3d). The urban-side mountain downslope wind accelerates while descending through a thin layer (Fig. 3d). Around 1800 LST, a hydraulic jump starts to occur near the mountain–urban edge when the strong and thin downslope wind merges with the urban wind. Additionally, the larger roughness length in the urban area contributes partly to the development of this hydraulic jump. The upward motion in association with the hydraulic jump has a maximum intensity of 1 m s^{-1} at 2000 LST, and afterward the hydraulic jump begins to weaken and eventually disappears.

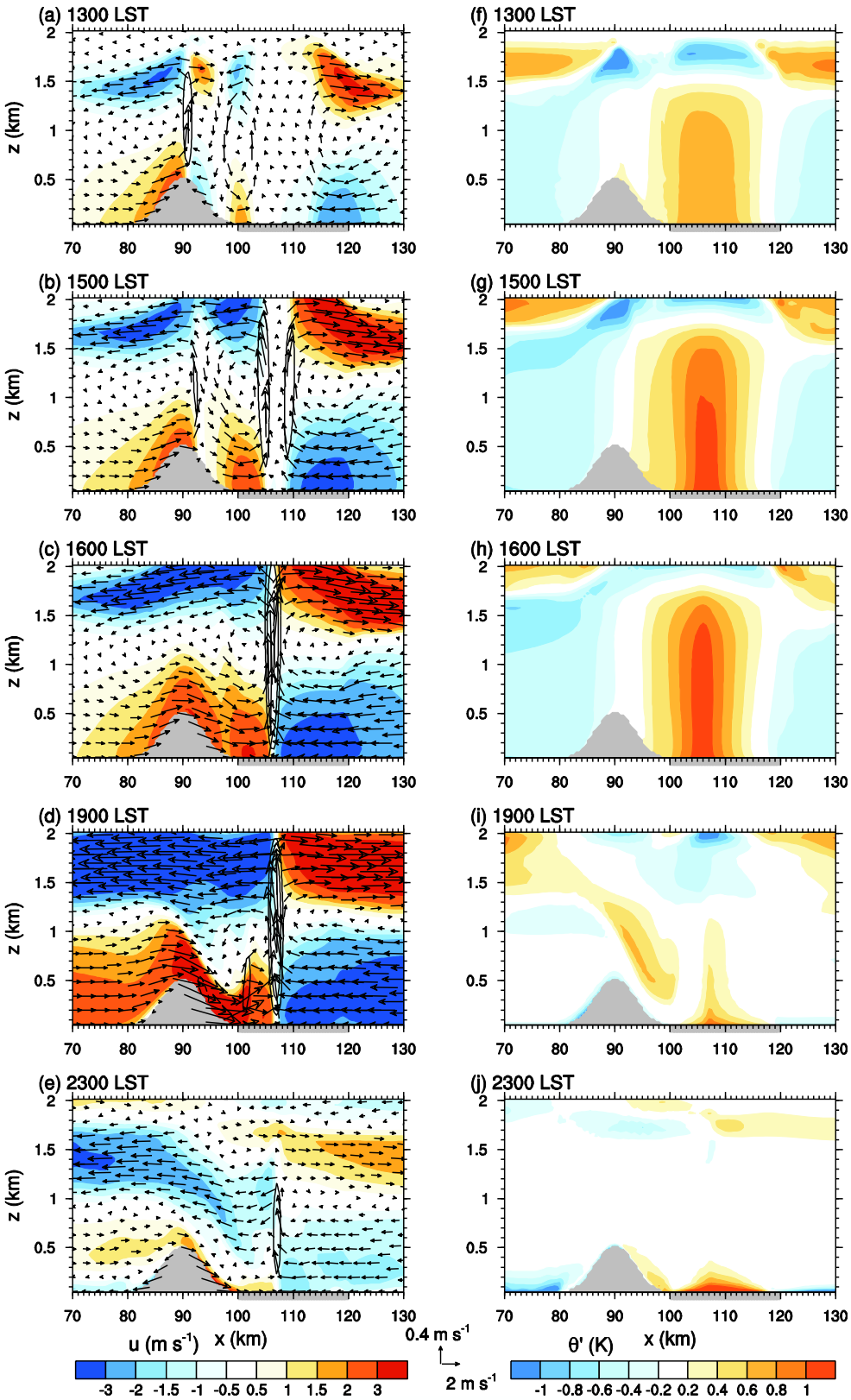

Fig. 3 Horizontal velocity (*shading*), vertical velocity (*contour*), and velocity vector fields at **a** 1300, **b** 1500, **c** 1600, **d** 1900, and **e** 2300 LST and corresponding potential temperature anomaly field (*shading*) at **f** 1300, **g** 1500, **h** 1600, **i** 1900, and **j** 2300 LST in the URBAN-MOUNT simulation. The *gray box on the x-axis* indicates the urban area. The contour levels of vertical velocity are −0.5 (*dashed line*, **d**), 0.5, 1, and 2 m s^{-1}

A simulation was performed with the hydrostatic mode of the WRF model. It was revealed that a hydraulic jump also occurs in the hydrostatic mode but with later onset, weaker intensity, and shorter presence period. Since the hydraulic

jump is an interesting phenomenon, we plan to study deep into its occurrence conditions and occurrence mechanisms through extensive numerical simulations and analyses.

Savijarvi and Liya (2001) demonstrated that urban breeze circulation opposes the weak daytime upslope circulation of a narrow valley. Similarly, Ohashi and Kida (2002) showed that in the daytime the weakening of winds toward urban and mountain areas is caused by their opposing wind directions. In essence, the results of the present study are consistent with those of both Savijarvi and Liya (2001) and Ohashi and Kida (2002).

The combined effects of the city and mountain on the local wind system produce some interesting features, including an earlier transition from upslope wind to downslope wind on the urban-side mountain slope and a stronger downslope wind. At the midslope location of the urban-side mountain slope, the transition from upslope wind to downslope wind occurs around 1430 LST, which is approximately 4 h earlier than the transition in the MOUNT simulation. The rural-side upslope wind passes over the mountain top, and the urban-side downslope wind is enhanced (Fig. 3c, d). The combined effects of the city and mountain also produce an extended period of urban-side downslope wind. The occurrence frequency of downslope wind at the urban-side midslope location constitutes 68 % of total wind during the 24-h period.

Figure 4 shows the distance–time section of 10-m horizontal wind in the URBAN, MOUNT, and URBAN-MOUNT simulations. Note that the mountain and city span x=80–100 km and x=100–120 km, respectively. The urban breeze is weaker, and its horizontal extent is smaller in the nighttime than in the daytime (Fig. 4a). Around 1635 LST, the urban breeze reaches its maximum intensity of 2.9 m s^{-1} at x=103 and 117 km. The horizontal extension and intensity of downslope wind are smaller and weaker, respectively, than those of upslope wind (Fig. 4b). Around 1840 LST, the transition from upslope wind to downslope wind begins near the mountain top. The downslope wind reaches its maximum intensity of 1.5 m s^{-1} around 1925 LST, and the upslope wind starts again around 0650 LST.

In the URBAN-MOUNT simulation, asymmetric winds over the urban area appear owing to the combined effects of the city and mountain (Fig. 4c). The onset of the mountain-side urban breeze is delayed by about 2 h with respect to that of the plain-side urban breeze. The transition from upslope wind to downslope wind on the urban-side mountain slope occurs earlier than that on the rural-side mountain slope. The maximum downslope wind speed at the urban-side midslope location (4.2 m s^{-1}) is roughly twice the maximum downslope wind at the rural-side midslope location (1.9 m s^{-1}). Moreover, the plain-side urban wind in the URBAN-MOUNT simulation is slightly stronger than that in the URBAN simulation. In the nighttime, the urban wind is slightly stronger in the URBAN-MOUNT simulation than in the URBAN simulation and the downslope wind is slightly stronger in the URBAN-MOUNT simulation than in the MOUNT simulation.

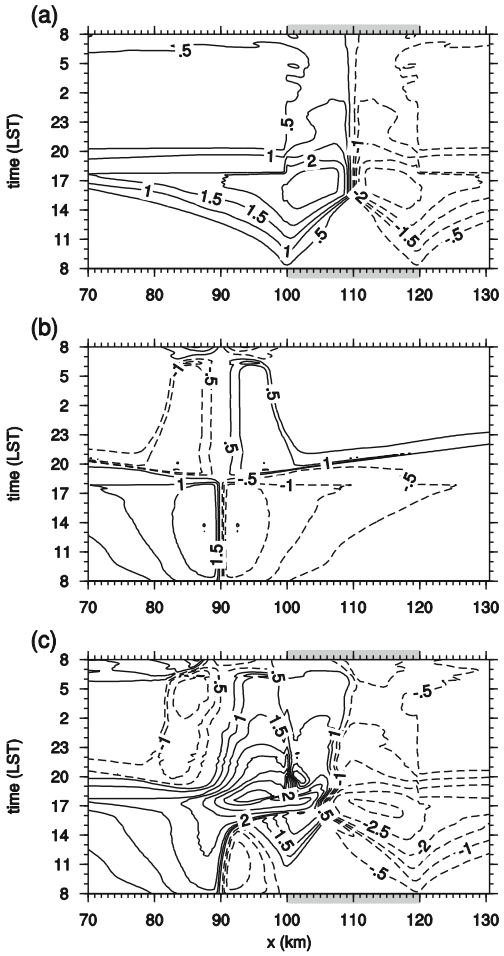

Fig. 4 Distance–time section of horizontal wind at 10 m above the surface in the **a** URBAN, **b** MOUNT, and **c** URBAN-MOUNT simulations. The *gray box on the x-axis* indicates the urban area. The mountain is located in the region from x=80 to 100 km in **b** and **c**. The contour intervals are 0.5 m s^{-1}

The vertical profiles of potential temperature at x=110 km in the URBAN, MOUNT, and URBAN-MOUNT simulations are presented in Fig. 5 for 1600 LST. A well-mixed boundary layer is produced. The boundary layer height in the URBAN (~2,430 m) and URBAN-MOUNT (~2,340 m) simulations is higher than that in the MOUNT simulation (~1,730 m) owing to stronger surface sensible heat flux in the presence of the city. The potential temperature near z=2 km is higher in the URBAN-MOUNT simulation than in the URBAN simulation, although the potential temperature profiles for these simulations are generally very similar.

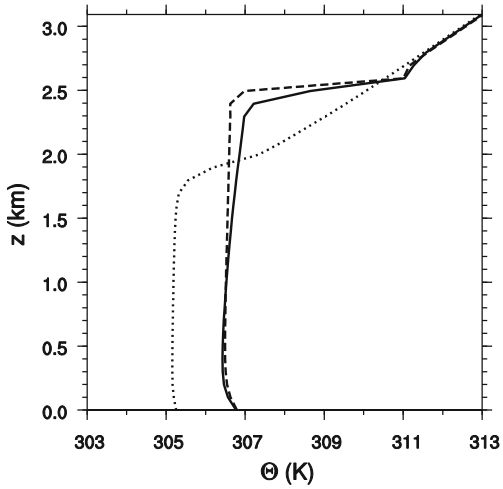

Fig. 5 Vertical profiles of potential temperature at x=110 km and t=1600 LST in the URBAN (*dashed*), MOUNT (*dotted*), and URBAN-MOUNT (*solid*) simulations

3.3 Sensitivity to mountain height and urban fraction

The effects of mountain height and urban fraction on interactions between urban breeze circulation and mountain slope winds and urban heat island intensity are examined here, based upon sensitivity experiments conducted for various maximum mountain heights and urban fractions in the presence of both a city and a mountain.

Figure 6 shows the horizontal velocity, vertical velocity, and velocity vector fields at 1500 LST in simulations with maximum mountain heights of 300, 500, 700, and 900 m. The mean slope angles of mountains are 1.7°, 2.8°, 3.9°, and 5.1°, respectively, for maximum mountain heights of 300, 500, 700, and 900 m. The 500-m case is the URBAN-MOUNT simulation case (Section 3.2). The experimental setup and parameter values in the other three cases are the same as those in the URBAN-MOUNT simulation but for maximum mountain height (h_m). As mountain height increases, the rural-side upslope wind weakens slightly but exists longer. In the simulation with h_m=300 m, the downslope wind is evident on the urban-side mountain slope (Fig. 6a). The urban-side downslope wind in the simulation with h_m=300 m is much stronger than that in the simulation with h_m=500 m (Fig. 6a, b). In the simulations with h_m=700 and 900 m, the upslope wind and downslope wind coexist on the urban-side mountain slope, with stronger upslope wind in the upper slope region and weaker downslope wind in the lower slope region in the h_m=900 m simulation than in the h_m=700 m simulation (Fig. 6c, d). These features likely occur because the urban effect becomes more important than the mountain effect at 1500 LST as mountain height decreases. Lee and Kimura (2001) demonstrated that anabatic winds strengthen as mountain height increases and that mountain height is one of the major factors affecting the temporal evolution of predominant mesoscale circulation over inhomogeneous land surfaces and non-uniform terrain. In the present study, the plain-side urban wind intensifies slightly as mountain height increases (Fig. 6). In the simulation with h_m=900 m, the updraft cell lies immediately over the mountain top. Two updraft cells over the urban area, which are associated with the two urban breeze fronts, are located further toward the mountain as mountain height increases. This is likely related to the stronger plain-side urban wind that occurs in the simulations with greater mountain heights.

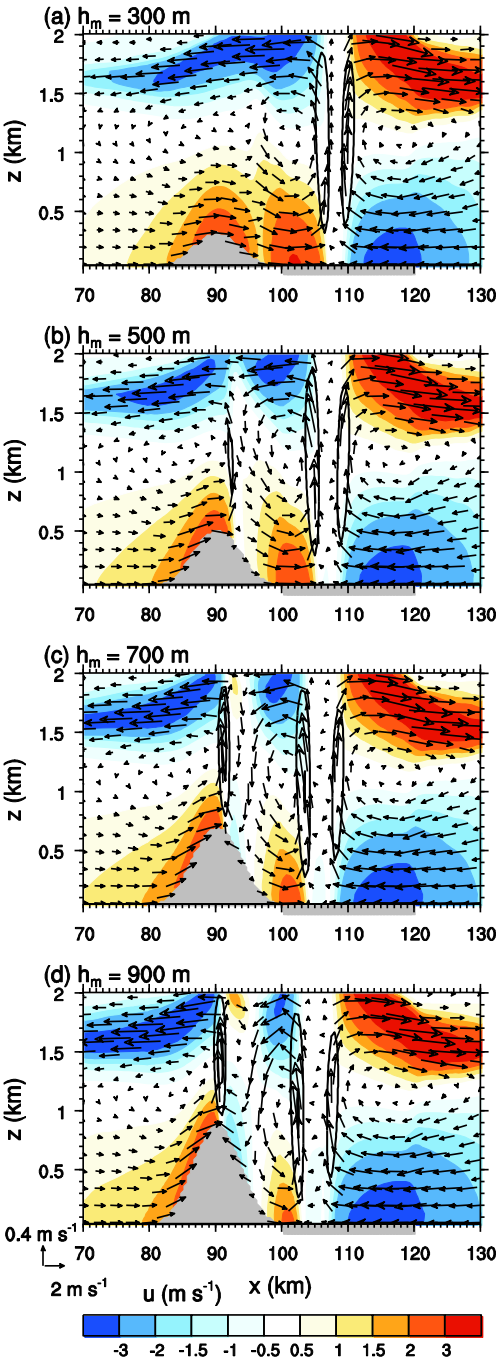

Fig. 6 Horizontal velocity (*shading*), vertical velocity (*contour*), and velocity vector fields at 1500 LST in the simulations with maximum mountain heights of **a** 300, **b** 500, **c** 700, and **d** 900 m. The contour levels of vertical velocity are 0.5 and 1 m s^{-1}

The horizontal velocity, vertical velocity, and velocity vector fields at 1500 LST in simulations with urban fractions of 0.2, 0.4, 0.6, and 0.8 are presented in Fig. 7. The 0.8 case is the URBAN-MOUNT simulation case (Section 3.2). The experimental setup and parameter values in the other three cases are the same as those in the URBAN-MOUNT simulation but for urban fraction (f_u). As urban fraction increases, the urban breeze circulation intensifies owing to stronger sensible heat flux. This is consistent with the results of Zhang et al. (2014).

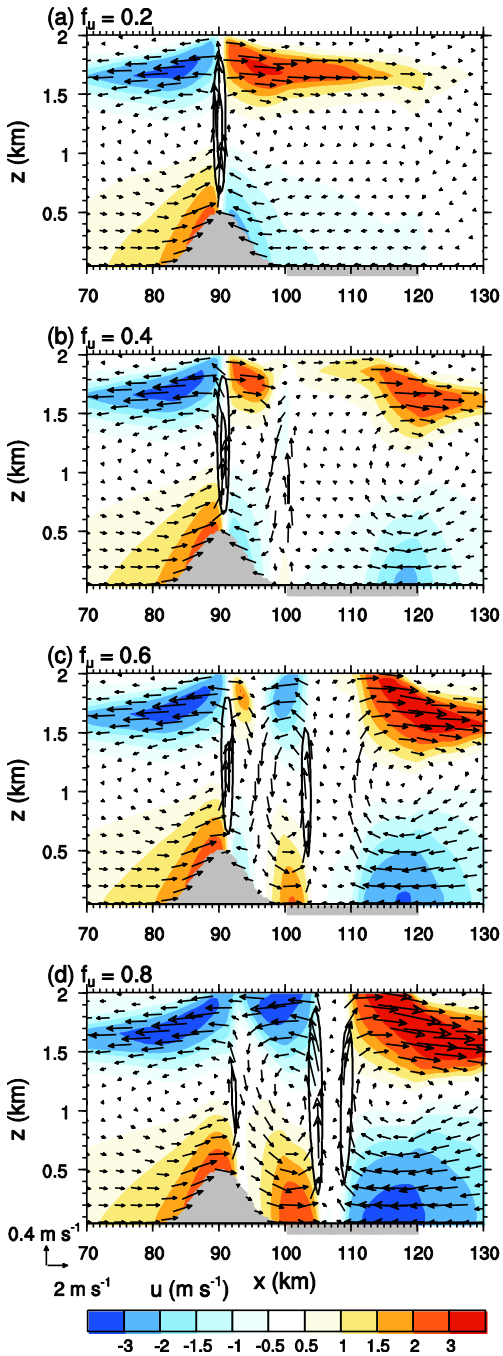

Fig. 7 Same as in Fig. 6 but for the simulations with urban fractions of **a** 0.2, **b** 0.4, **c** 0.6, and **d** 0.8

In the simulation with f_u=0.8, the urban wind is stronger than that in the simulation with f_u=0.6. In the simulations with f_u=0.6 and 0.8, the upslope wind and downslope wind coexist on the urban-side mountain slope, with stronger downslope wind in the lower region and weaker upslope wind in the upper region in the simulation with f_u=0.8 than in the simulation with f_u=0.6. These features likely occur because the mountain effect becomes more important than the urban effect at 1500 LST as urban fraction decreases. The rural-side upslope wind tends to accelerate slightly in the upper slope region with increasing urban fraction (Fig. 7). In the simulations with f_u=0.6 and 0.8, the updraft cells with vertical velocity greater than 0.5 m s^{-1} are evident over the urban area (Fig. 7c, d). The updraft cell over the mountain top weakens and moves slightly toward the urban-side slope as urban fraction increases.

Extensive numerical experiments are conducted to examine the dependencies of urban wind and slope winds on mountain height and urban fraction. To achieve this, maximum mountain height is varied from 100 to 1,000 m at intervals of 100 m and urban fraction is varied from 0.2 to 0.9 at intervals of 0.1; this results in 80 simulations. Figure 8 shows the transition time from upslope wind to downslope wind and the percentage of occurrence frequency of downslope wind at the urban-side midslope location (x=95 km) and the horizontal winds at the mountain–urban edge (x=100 km) and the urban–rural edge (x=120 km) as a function of maximum mountain height and urban fraction. The horizontal winds at the mountain–urban and urban–rural edges are averaged over the period 0800–2000 LST, and the percentage of the occurrence frequency of downslope wind at x=95 km is over a 1-day period spanning 0800–0800 LST.

The transition from upslope wind to downslope wind starts earlier as mountain height decreases and urban fraction increases (Fig. 8a). The transition time exhibits a greater dependency on mountain height when urban fraction is larger. The simulation with the highest mountain (h_m=1,000 m) and smallest urban fraction (f_u=0.2) exhibits the latest transition from upslope wind to downslope wind, which occurs at 1835 LST. Conversely, the simulation with the lowest mountain (h_m=100 m) and largest urban fraction (f_u=0.9) shows the earliest transition, which occurs at 1125 LST. This change in transition time influences interactions between urban breeze circulation and mountain slope winds.

The occurrence frequency (%) of downslope wind at the urban-side midslope location during the 1-day period increases as mountain height decreases and urban fraction increases (Fig. 8b). The occurrence frequency of downslope wind is more sensitive to urban fraction when mountain height is lower. When urban fraction is smaller, the occurrence frequency of downslope wind has a smaller sensitivity to mountain height. The occurrence frequency of upslope wind is similar to that of downslope wind when urban fraction is

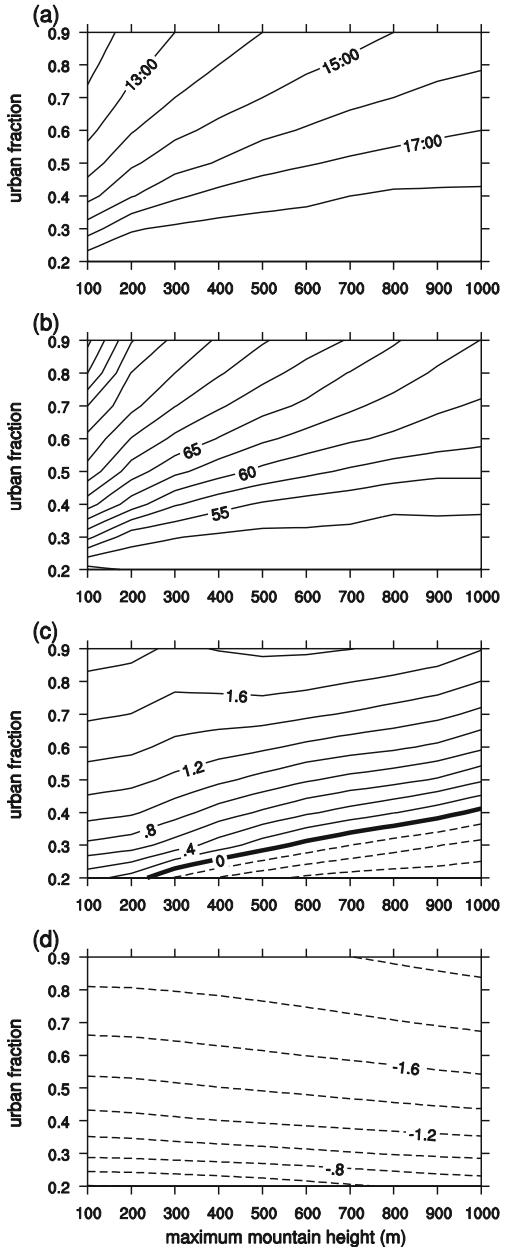

Fig. 8 **a** Transition time from upslope wind to downslope wind (at 10 m above the slope) at the urban-side midslope location (x=95 km), **b** percentage of the occurrence frequency of downslope wind (at 10 m above the slope) at the urban-side midslope location, and 10-m horizontal wind at **c** the mountain–urban edge (x=100 km) and **d** the urban–rural edge (x=120 km) as a function of maximum mountain height and urban fraction. **c** and **d** are averaged over the period 0800–2000 LST, and **b** is for the 1-day period 0800–0800 LST. The contour intervals in **a**, **b**, **c**, and **d** are 1 h, 2.5 %, 0.2 and 0.2 m s^{-1}, respectively

very small. In the simulation with the lowest mountain and largest urban fraction, the downslope wind consists of 85 % of total wind according to its occurrence frequency.

The averaged 10-m horizontal wind at the mountain–urban edge is toward the urban or mountain area depending on mountain height and urban fraction (Fig. 8c). The strongest wind toward the mountain area (0.8 m s^{-1}) occurs in the simulation with the highest mountain and smallest urban fraction, whereas the strongest wind toward the urban area (1.8 m s^{-1}) occurs in the simulation with the lowest mountain and largest urban fraction. Each urban fraction increase of 0.1 results in an average increase of 0.3 m s^{-1} in the speed of wind toward the urban area. Each maximum mountain height increase of 100 m results in an average increase of 0.1 m s^{-1} in the speed of wind traveling toward the mountain area.

The averaged 10-m horizontal wind at the urban–rural edge strengthens as mountain height increases and urban fraction increases (Fig. 8d). The dependency of the horizontal wind on mountain height is small for a given urban fraction, whereas the dependency of the horizontal wind on urban fraction for a given mountain height is relatively large. The horizontal wind is strongest (2.1 m s^{-1}) in the simulation with the highest mountain and largest urban fraction and weakest (0.4 m s^{-1}) in the simulation with the lowest mountain and smallest urban fraction. Here, each urban fraction increase of 0.1 results in an average increase of 0.2 m s^{-1} in the plain-side urban wind.

Figure 9 shows the daytime- and nighttime-averaged urban heat island intensities as a function of maximum mountain height and urban fraction. Here, the urban heat island intensity is calculated as the difference in 2-m air temperature averaged over x=100–120 km between any case with given maximum mountain height and urban fraction and the case with homogeneous surface and uniform terrain (no city and no mountain). The daytime and nighttime averages are taken from 1200 to 1700 LST and from 0000 to 0500 LST, respectively. As expected, the urban heat island is stronger in the nighttime

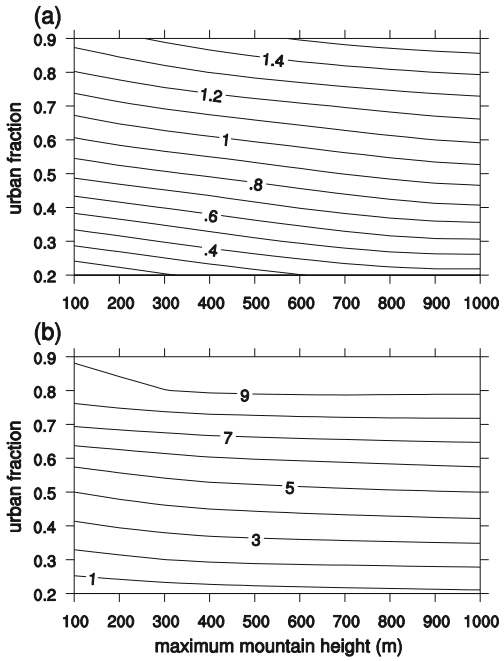

Fig. 9 **a** Daytime (1200–1700 LST) and **b** nighttime (0000–0500 LST) averaged urban heat island intensities as a function of maximum mountain height and urban fraction

than in the daytime. In both the daytime and nighttime, the sensitivity of urban heat island intensity to urban fraction is more significant than that to maximum mountain height. The daytime urban heat island intensity increases as mountain height increases and urban fraction increases. In the nighttime, the dependency of urban heat island intensity on urban fraction is considerably large for a given maximum mountain height. The nighttime urban heat island intensity for a given urban fraction varies very little with mountain height when maximum mountain height is greater than about 500 m. Each urban fraction increase of 0.1 results in average increases of 0.17 and 1.27 °C in the daytime and nighttime urban heat island intensities, respectively.

3.4 A city in a basin

This section presents the results of a simulation in which a city is located in a basin between two isolated mountains (the BASIN simulation). In this case, the urban center coincides with the domain and basin centers, two identical mountains have maximum heights of 500 m, and the urban fraction is 0.8.

Figure 10 shows the horizontal velocity, vertical velocity, and velocity vector fields at 1200, 1500, 1600, 1900, and 2300 LST in the BASIN simulation. The circulation developed is symmetric about the city center. At 1200 LST, the plain-side upslope wind and the return flow over the plain side are stronger and deeper than those over the basin side owing to the weakened urban-side upslope wind that is associated with the opposing urban breeze. The urban-side upslope wind reaches a maximum intensity of 1.9 m s^{-1} around 1025 LST. At the urban-side midslope location, the downslope wind starts around 1400 LST. This downslope wind facilitates the plain-to-basin wind. The earlier onset of plain-to-basin wind in the present study is distinct from the results of previous studies adopting homogeneous land surfaces (e.g., Kimura and Kuwagata 1993; de Wekker et al. 1998); such studies have suggested that the plain-to-basin wind commences at dusk. Valley geometry results in the accumulation of more heat than plain geometry (Kimura and Kuwagata 1995), thus producing lower pressure inside the valley than over the plain. At 1500 and 1600 LST, there are two updraft cells over the urban area. These cells move toward the urban center and merge around 1635 LST. The urban-side downslope wind attains a maximum intensity of 7.9 m s^{-1} around 1815 LST; this is stronger than the downslope wind on the urban-side slope in the URBAN-MOUNT simulation. At 1900 LST, a strong updraft cell appears over the urban center. As

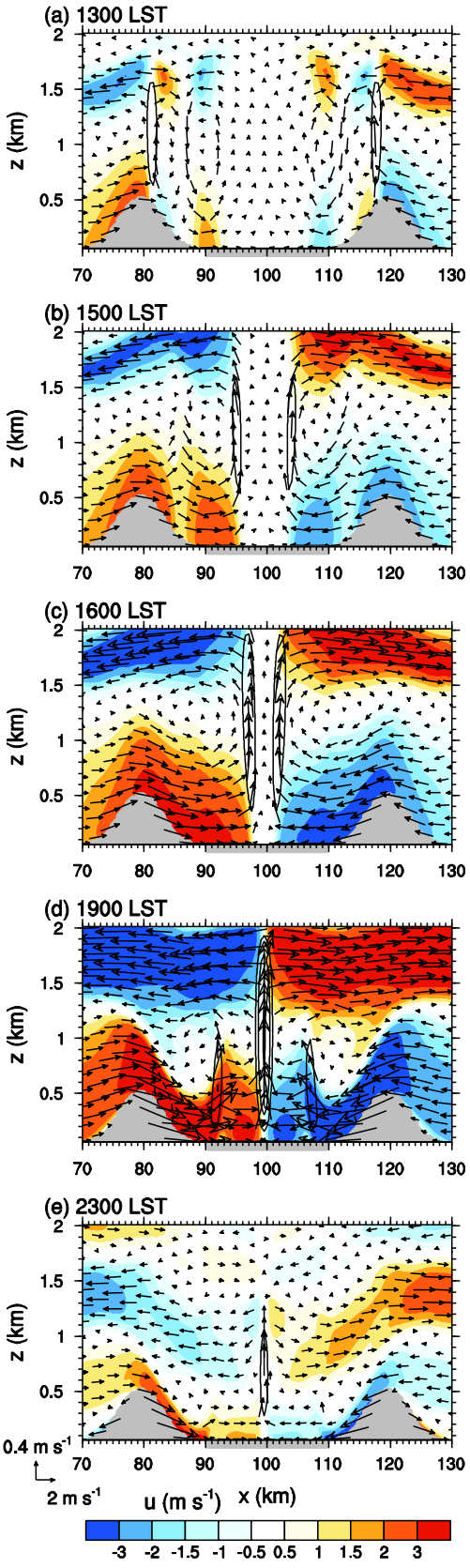

Fig. 10 Horizontal velocity (*shading*), vertical velocity (*contour*), and velocity vector fields at **a** 1200, **b** 1500, **c** 1600, **d** 1900, and **e** 2300 LST in the BASIN simulation. The *gray box on the x-axis* indicates the urban area. The contour levels of vertical velocity are −0.5 (*dashed line*, **d**), 0.5, 1, and 2 m s^{-1}

demonstrated in Kimura and Kuwagata (1993), the strong downslope wind on the basin-side mountain slope around

sunset or after dusk is owing to the plain-to-basin wind as well as the downslope wind. The transition time from upslope wind to downslope wind at the rural-side midslope location in the BASIN simulation is almost the same as that in the URBAN-MOUNT simulation. The urban-side downslope wind persists longer than the rural-side downslope wind. Around 1745 LST, hydraulic jumps occur near the mountain–urban edges. They persist until 2145 LST. The potential temperature anomaly over the urban area is smaller in the BASIN simulation than in the URBAN-MOUNT simulation (not shown). This is likely associated with stronger plain-to-basin wind from the plain areas in the BASIN simulation, which contributes to cooling of the basin air.

4 Summary and conclusions

The present study examined interactions between urban breeze circulation and mountain slope winds in two dimensions using the WRF model coupled with an advanced urban canopy model. Circulation over the urban area is characterized by the weakened mountain-side urban wind owing to the opposing upslope wind and the strengthened plain-side urban wind in the daytime. The transition from upslope wind to downslope wind on the urban-side slope starts earlier than that in a simulation that includes only an isolated mountain. A hydraulic jump is observed in the late afternoon and stagnates until late evening. Extensive numerical experiments were performed to examine the sensitivities of the interactions of urban breeze circulation with mountain slope winds and urban heat island intensity to mountain height and urban fraction. It was found that the transition from urban-side upslope wind to downslope wind starts earlier and that the urban-side downslope wind persists longer with decreasing mountain height and increasing urban fraction. The change in transition time from upslope wind to downslope wind affects interactions between urban breeze circulation and mountain slope winds. Urban heat island intensity was found to be more sensitive to urban fraction than to mountain height. Finally, a case in which a city is located in a basin between two identical mountains was examined. Here, the urban-side downslope wind develops earlier and persists longer than the rural-side downslope wind and the plain-to-basin wind is stronger than in the simulation that includes a city and an isolated mountain.

This study investigated the interactions of urban breeze circulation with mountain slope winds in two dimensions. In three dimensions, various shapes of urban heat island and mountain can be considered and more complex but more realistic interactions can be simulated. Thus, extension of the present study to three dimensions will be required to further improve understanding of the interactions between urban breeze circulation and mountain slope winds.

Acknowledgments The authors are grateful to two anonymous reviewers and Jaemyeong Mango Seo for providing valuable comments on this work. This work was funded by the National Research Foundation of Korea (NRF) grant funded by the Korea Ministry of Education, Science and Technology (MEST) (No. 2012-0005674).

References

Chen F, Dudhia J (2001) Coupling an advanced land surface–hydrology model with the Penn State–NCAR MM5 modeling system. Part I: model implementation and sensitivity. Mon Weather Rev 129:569–585

Chen SH, Sun WY (2002) A one-dimensional time dependent cloud model. J Meteorol Soc Jpn 80:99–118

de Wekker SFJ, Zhong S, Fast JD, Whiteman CD (1998) A numerical study of the thermally driven plain-to-basin wind over idealized basin topographies. J Appl Meteorol 37:606–622

Dudhia J (1989) Numerical study of convection observed during the winter monsoon experiment using a mesoscale two-dimensional model. J Atmos Sci 46:3077–3107

Fernando HJS (2010) Fluid dynamics of urban atmospheres in complex terrain. Annu Rev Fluid Mech 42:365–389

Hidalgo J, Masson V, Pigeon G (2008a) Urban-breeze circulation during the CAPITOUL experiment: numerical simulations. Meteorol Atmos Phys 102:243–262

Hidalgo J, Pigeon G, Masson V (2008b) Urban-breeze circulation during the CAPITOUL experiment: observational data analysis approach. Meteorol Atmos Phys 102:223–241

Hong SY, Noh Y, Dudhia J (2006) A new vertical diffusion package with an explicit treatment of entrainment processes. Mon Weather Rev 134:2318–2341

Kimura F, Kuwagata T (1993) Thermally induced wind passing from plain to basin over a mountain range. J Appl Meteorol 32:1538–1547

Kimura F, Kuwagata T (1995) Horizontal heat fluxes over complex terrain computed using a simple mixed-layer model and a numerical model. J Appl Meteorol 34:549–558

Lee SH, Kim HD (2010) Modification of nocturnal drainage flow due to urban surface heat flux. Asia-Pac J Atmos Sci 46:453–465

Lee SH, Kimura F (2001) Comparative studies in the local circulations induced by land-use and by topography. Bound-Layer Meteorol 101:157–182

Lemonsu A, Masson V (2002) Simulation of a summer urban-breeze over Paris. Bound-Layer Meteorol 104:463–490

Mlawer EJ, Taubman SJ, Brown PD, Iacono MJ, Clough SA (1997) Radiative transfer for inhomogeneous atmospheres: RRTM, a validated correlated-k model for the longwave. J Geophys Res 102:16663–16682

Ohashi Y, Kida H (2002) Effects of mountains and urban areas on daytime local-circulations in the Osaka and Kyoto regions. J Meteorol Soc Jpn 80:539–560

Pielke RA (2002) Mesoscale meteorological modeling, 2nd edn. Academic Press, San Diego

Ryu YH, Baik JJ (2013) Daytime local circulations and their interactions in the Seoul metropolitan area. J Appl Meteorol Climatol 52:784–801

Ryu YH, Baik JJ, Lee SH (2011) A new single-layer urban canopy model for use in mesoscale atmospheric models. J Appl Meteorol Climatol 50:1773–1794

Ryu YH, Baik JJ, Han JY (2013a) Daytime urban breeze circulation and its interaction with convective cells. Q J R Meteorol Soc 139:401–413

Ryu YH, Baik JJ, Kwak KH, Kim S, Moon N (2013b) Impacts of urban land-surface forcing on ozone air quality in the Seoul metropolitan area. Atmos Chem Phys 13:2177–2194

Savijarvi H, Liya J (2001) Local winds in a valley city. Bound-Layer Meteorol 100:301–319

Simpson JE (1994) Sea breeze and local winds. Cambridge University Press, New York

Skamarock WC, Klemp JB, Dudhia J, Gill DO, Barker DM, Duda MG, Huang XY, Wang W, Powers JG (2008) A description of the advanced research WRF version 3. NCAR, Boulder

Wong KK, Dirks RA (1978) Mesoscale perturbations on airflow in the urban mixing layer. J Appl Meteorol 17:677–688

Zhang N, Wang X, Peng Z (2014) Large-eddy simulation of mesoscale circulations forced in inhomogeneous urban heat island. Bound-Layer Meteorol 151:179–194